ACS APPLIED MATERIALS & INTERFACES

Research Article

www.acsami.org

Preparation of Rutile TiO_2 Coating by Thermal Chemical Vapor Deposition for Anticoking Applications

Shiyun Tang,[†] Jianli Wang,*[,†] Quan Zhu,[‡] Yaoqiang Chen,*[,†] and Xiangyuan Li[‡]

[†]Key Laboratory of Green Chemistry & Technology of the Ministry of Education, College of Chemistry, Sichuan University, Chengdu 610064, P. R. China

[‡]College of Chemical Engineering, Sichuan University, Chengdu 610065, P. R. China

ABSTRACT: To inhibit the metal catalytic coking and improve the oxidation resistance of TiN coating, rutile TiO_2 coating has been directly designed as an efficient anticoking coating for *n*-hexane pyrolysis. TiO_2 coatings were prepared on the inner surface of SS304 tubes by a thermal CVD method under varied temperatures from 650 to 900 °C. The rutile TiO_2 coating was obtained by annealing the as-deposited TiO_2 coating, which is an alternative route for the deposition of rutile TiO_2 coating. The morphology, elemental and phase composition of TiO_2 coatings were characterized by SEM, EDX and XRD, respectively. The results show that deposition temperature of TiO_2 coatings has a strong effect on the morphology and thickness of as-deposited TiO_2 coatings. Fe, Cr and Ni at.% of the substrate gradually changes to 0 when the temperature is increased to 800 °C. The thickness of TiO_2 coating is more than 6 μm and uniform by metalloscopy, and the films have a nonstoichiometric composition of Ti_3O_8 when the deposition temperature is above 800 °C. The anticoking tests show that the TiO_2 coating at a deposition temperature of 800 °C is sufficiently thick to cover the cracks and gaps on the surface of blank substrate and cut off the catalytic coke growth effect of the metal substrate. The anticoking ratio of TiO_2 coating corresponding to each 5 cm segments is above 65% and the average anticoking ratio of TiO_2 coating is up to 76%. Thus, the TiO_2 coating can provide a very good protective layer to prevent the substrate from severe coking efficiently.

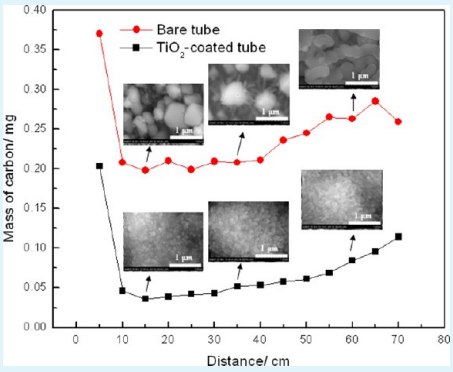

KEYWORDS: *oxidation resistance, rutile TiO_2, anticoking coating, n-hexane pyrolysis, anticoking ratio*

1. INTRODUCTION

Titanium dioxide (TiO_2) has three polymorphs in nature: anatase, rutile, and brookite. In the past three decades, TiO_2 coatings have been widely studied in dye-sensitized solar cell,[1] photoelectrochemistry,[2] photocatalysis,[3] and thin film electronic devices,[4] etc. In these applications, an anatase TiO_2 is often broadly used thanks to its chemical stability, excellent mechanical durability, high refractive index, and transparency over the wide spectral range. Rutile is the only stable phase at high temperature, whereas anatase and brookite are metastable at all temperatures and transform to rutile if they are heated. Rutile TiO_2 coating is seldom investigated although it exhibits thermal stability, high hardness, and high Young's modulus value as compared with anatase and brookite. Yin et al. reported the rutile TiO_2 coating layer on lamellar sericite surface by the chemical deposition method starting from $TiCl_4$ in the presence of Sn^{4+} which induced the TiO_2 phase transformation of amorphous to rutile.[5] Luo et al. studied the structure and mechanical properties of thick rutile TiO_2 films under different coating treatments.[6] Recently, there is increasing interest in the use of various thin films or coatings as anticoking coatings during hydrocarbon pyrolysis at high temperature, such as glass coating,[7] Al_2O_3 coating,[8,9] SiO_2/S coating,[10−12] Ta_2O_5 coating,[9] and TiN coating.[13] Anticoking coating is to solve the metal dusting and coking problems, wherein metal dusting is a serious carburization of Fe-, Ni-, and Co-base alloys which not only leads to disintegration of the metal substrate to small metal particles leaving pits and grooves, but also causes severe catalytic coking further. This phenomenon often occurs in the process of hydrocarbon pyrolysis at high temperature, accompanied by the formation of carbonaceous solid deposits (also known as coke) on the metal surface, thereby worsen the heat transfer process by sharply increasing heat resistances and weaken the substrate. In our previous works, TiN coatings has been designed as anticoking coatings during hydrocarbon fuels pyrolysis under high temperature and pressure, and the results have shown that TiN coating provides a good protective layer to prevent the substrate from severe coking.[13−15] However, there is often dozens to hundreds of parts per million dissolved O_2 in hydrocarbon fuels,[16] which will cause the formation of oxygenated products and the oxidation of TiN coating. On the other hand, the oxidation resistance of TiN is very poor under the high temperature, and the oxidation of TiN into rutile TiO_2 often starts between 500 and 600 °C.[17−20] Therefore, in this work, a stable phase of rutile TiO_2 coating has been directly considered as anticoking coating during hydrocarbon pyrolysis.

Received: July 23, 2014
Accepted: September 5, 2014
Published: September 5, 2014

Several techniques have been used for the synthesis of TiO_2 coatings including sol−gel synthesis,[21] hydrolytic precipitation,[22] spray coating,[23] sputtering,[24] and chemical vapor deposition (CVD) method.[25] Wherein CVD method is one of the most popular synthesis methods due to the easily controlled of processing and high-quality crystalline thin films. Kaliwoh et al.[26] prepared anatase TiO_2 thin films on crystalline Si and quartz by photoinduced CVD method. Lei et al.[27] reported that two kinds of metal organic CVD approaches were employed for the preparation of the photocatalyst of TiO_2 supported on alumina. Guo et al.[28] employed laser CVD method to prepare TiO_2 coating on $Pt/Ti/SiO_2/Si$ substrate. Nevertheless, only a few studies were found on the deposition of TiO_2 coatings by thermal CVD. Typically, Sun et al.[29] prepared TiO_2 films on glass in a vertical quartz glass chamber at deposition temperature between 300 and 600 °C under atmospheric pressure by thermal CVD where $TiCl_4$ was used as the precursor to react with H_2O vapor. Fredriksson and Carlsson[30] investigated the thermal CVD deposition of TiO and Ti_2O_3 from $TiC1_4/H_2/CO_2$ gas mixtures under 1000 °C and pressures in the range of $(13-6.7) \times 10^3$ Pa. In this paper, to obtain a good anticoking coating without affecting the performance of substrate, TiO_2 coating was prepared on nonplanar metal substrate at relatively low temperature (below 900 °C) by thermal CVD.

We will present in this paper an alternative route for the preparation of rutile TiO_2 coating. The microstructure, elemental, and phase composition of TiO_2 coatings will be examined. Then we will show how the coking activity can be suppressed by rutile TiO_2 coating during the hydrocarbon fuel pyrolysis process under high temperature and pressure, and how these observations can help to obtain the optimal deposition conditions for anticoking rutile TiO_2 coating.

2. EXPERIMENTAL SECTION

2.1. Preparation of Rutile TiO_2 Coating. TiO_2 coatings were prepared on the inner surface of stainless steel 304 (SS304) tubes (3 mm o.d., 2 mm i.d. and 700 mm long) in a horizontal hot-wall type chamber (uniform temperature zone of 1000 mm) at atmospheric pressure using $TiCl_4-H_2-CO_2$ system. Titanium tetrachloride ($TiCl_4$) with a purity of 99.0% was used as the precursor which was purchased from Chengdu Kelong Chemical Reagent Company. The main elemental composition in atomic percentage (at.%) of SS304 substrate used in this study is 20.8% for Cr, 7.4% for Ni, and 71.8% for Fe, and more details were described elsewhere.[14] The thermal CVD deposition process of TiO_2 coatings from $TiC1_4/H_2/CO_2$ gas mixtures comprises two homogeneous gas-phase reactions that can be described by the following chemical reactions

$$CO_2(g) + H_2(g) \rightarrow CO(g) + H_2O(g) \quad (1)$$

$$2H_2O(g) + TiCl_4(g) \rightarrow TiO_2(s) + 4HCl(g) \quad (2)$$

Where the (s) means solid phase and (g) means gas phase. Eq 1 is the homogeneous "water gas shift" reaction to in situ produce the water used in the hydrolysis reaction. This reaction was investigated comprehensively by Tingey,[31] who even gave the following water formation rate above 800 °C

$$d[H_2O]/dt = 7.6 \times 10^4 e^{-78000/RT}[H_2]^{1/2}[CO_2] \quad (3)$$

Then $TiCl_4$ reacted with H_2O vapor as shown in eq 2.

The apparatus of thermal CVD TiO_2 coatings is schematically described in Figure 1. Before deposition, the SS304 tubes were washed in soap solution, rinsed with acetone and ethanol, and then dried in a vacuum drying oven at 120 °C for an hour. In the process of heating period (usually 2.5−3 h), high purity (HP) N_2 mixed with a small amount of HP-H_2 was passing through the reaction system to purge the air inside and protect the substrate. After reaching the designed temperature, the $TiCl_4$ vapor with an equilibrium vapor pressure of 1.33 KPa at 21 °C was carried by purified HP-H_2, then through the gas mixing vessel to mix with H_2 and CO_2 fully, and eventually reached the surface of the substrate in sedimentary chamber where the deposition experiments were started. In this study, various substrate temperatures ranging from 650 to 900 °C were employed for TiO_2 coatings, and the deposition time was fixed at 3 h in each deposition. The flow rates of the carrier gas H_2, reactant H_2 and CO_2 were 1200, 1100, and 50 mL/min, respectively. The estimated $TiCl_4$ flow rate was 16 mL/min. To get a rutile TiO_2 coating, the as-deposited TiO_2 was annealed for 30 min in air conditions after cooling down to 700 °C. The annealing process can make the metastable phase of titanium oxides transform into thermodynamically stable phase of rutile TiO_2.

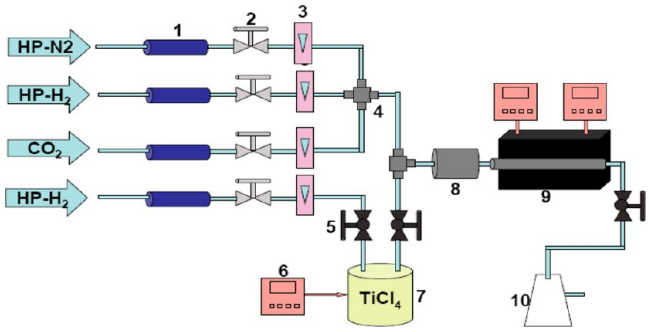

Figure 1. Schematic diagram of thermal CVD apparatus: 1, drying tube; 2, needle valve; 3, gas flowmeter; 4, union joint; 5, ball valve; 6, temperature controller; 7, $TiCl_4$ evaporator; 8, gas mixing vessel; 9, reaction chamber; 10, purification plant.

2.2. Anticoking Performance of TiO_2 Coating. The thermal cracking of *n*-hexane under high temperature and pressure was employed to evaluate the anticoking performance of TiO_2 coating. The experiments were carried out in a self-made supercritical cracking device which is shown in Figure 2. Unlike previous work,[14] here we made slight changes that two sections of heating mode were employed, which included a preheating section and an isothermal section (As shown in Figure 3). The outlet oil temperatures for both preheating section and isothermal section were controlled exactly the same. The main purpose of the added preheating section was to distinguish deposits formation between thermal oxidation coking and cracking coking. The coke formed by thermal oxidation can be removed in the preheating section so that only cracking coke formed in the isothermal section. The thermal cracking experiments were conducted in bare and annealed TiO_2-coated SS304 tubes (Both preheating section and isothermal section were 2 mm inside diameter and 700 mm long), and the conditions are given in Table 1 which included the cracking temperatures and pressures. The reactor was heated directly by electricity under the fixed pressure of the system with the aid of a backpressure controlling valve that was used to keep the system pressure constant. The fuel outlet temperature was measured by K-type thermocouples, and the wall temperatures were also measured by K-type thermocouples welded outside of the tube. At the end of the reactor, the cracking products were first cooled in the condenser and then flowed into a gas−liquid separator through the backpressure controlling valve. After thermal cracking experiments, the residual fuel in system was removed by HP-N_2, and the reactors were dried in a vacuum oven at 120 °C for 1h.

2.3. Analysis Method. The morphology and elemental composition of as-deposited TiO_2 coatings were characterized by scanning electron microscopy (SEM, Hitachi-S-4800, Japan) and energy dispersive X-ray spectroscopy (EDX, Oxford-IE-250, Germany), respectively. The thickness of TiO_2 coatings was measured by metalloscopy after embedding the TiO_2-coated tubes into resin and then cutting into slices, and the cross sections of 100 mm away from the gas inlet of TiO_2-coated tubes were typically chosen. The phase

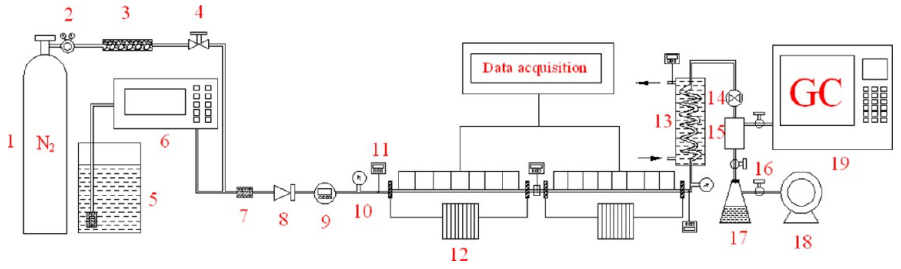

Figure 2. Flow reactor device for thermal cracking experiments with fuels: (1) N_2 cylinders; (2) relieve valve; (3) drying tube; (4) needle valve; (5) storage tanks; (6) high-performance liquid chromatograph; (7) filter; (8) nonreturning valve; (9) mass flowmeter; (10) pressure gauge; (11) thermocouple; (12) transformer; (13) condenser; (14) back-pressure valve; (15) gas/liquid separator; (16) ball valve; (17) liquid collector; (18) wet type gas flowmeter; (19) gas chromatograph (GC).

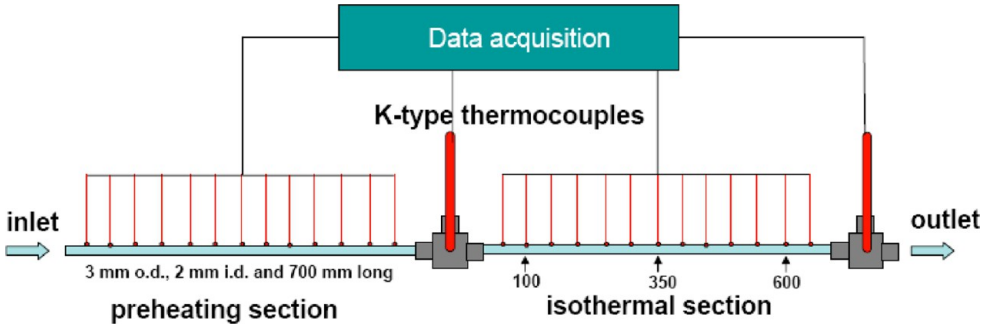

Figure 3. Schematic diagram of the electric heat tube reactor for *n*-hexane thermal cracking (conditions: temperature, 600 °C; pressure, 3.3 MPa; flow rate, 40 mL/min).

Table 1. Conditions Used to Thermal Cracking Experiments of *n*-Hexane

	bare tube		TiO_2-coated tube	
sample	preheating section	isothermal section	preheating section	isothermal section
fuel outlet temperature/T_{out} (°C)	600	600	600	600
reactor pressure (MPa)	3.3	3.3	3.3	3.3
flow rate (mL/min)	40	40	40	40
heating rate (°C/min)	100	100	100	100
experimental period (min)	60	60	60	60

composition of as-deposited and annealed TiO_2 coating was investigated by using X-ray diffraction (XRD). XRD experiment of the TiO_2 coating was carried out in a DX-2500 rotating anode X-ray diffractometer (Dandong Fangyuan Instruments Co., Ltd., China) using Cu *Ka* (λ = 0.15406 nm) radiation. The tube voltage and current were 40 kV and 100 mA, respectively. The X-ray diffractogram was recorded at 0.03 °/s intervals in the range of 20−80 °.

The coked bare and TiO_2-coated tubes were cut into 2 cm segments and three split segments were sampled: 100, 350, and 600 mm along the axial length of bare or coated tubes (see Figure 3), and the corresponding morphologies and micro zone amounts of carbonaceous deposits were characterized by SEM and EDX, respectively. The mass of coke on the surface of bare and TiO_2-coated tubes were obtained after thermal cracking of *n*-hexane at 600 °C and 3.3 MPa for 1h by temperature-programmed oxidation (TPO) in a CO_2 infrared analyzer. Before the TPO tests, the coked tubes were washed 3 times with pentane to remove any residual fuel, and then cut into 5 cm segments, washed again with pentane, and dried in a vacuum oven at 120 °C overnight to ensure the complete removal of the residual pentane. In the infrared analyzer, the coke was oxidized to CO_2 by HP-O_2 in a furnace and over a Pt/Al_2O_3 oxidation catalyst bed at 300 °C (CO was completely converted CO_2). The coked tube samples were loaded in a quartz reactor with flowing O_2 (2400 mL/min) and then burned at a fixed temperature of 900 °C. The product CO_2 was quantitatively measured by a calibrated infrared detector and used to calculate the carbon mass of coke. The anticoking ratio of the TiO_2 coating was calculated as follows

$$\text{anticoking ratio} = \frac{M - m}{M} 100\% \quad (4)$$

Where the M is the carbon mass of coke on the bare tube and m is the carbon mass of coke on the TiO_2-coated tube. The total carbon mass of coke measured on different tube surfaces is reproducible to within 3 wt % deviation of the deposit mass.

3. RESULTS AND DISCUSSION

3.1. Morphologies of As-Deposited TiO_2 Coatings. SEM images (2000:1) of as-deposited TiO_2 coatings (100 mm away from gas inlet) produced by thermal CVD at various deposition temperatures are shown in Figure 4. The apparent result is that the morphologies of as-deposited TiO_2 coatings are significantly changed as the deposition temperatures increased. Small particles and island structures with many cracks and gaps can be seen on the surface of as-deposited TiO_2 coating at a deposition temperature of 650 °C (Figure 4a). Irregular platelike crystals appear at the deposition temperatures of 700 and 750 °C (Figure 4b, c). Rice-shaped crystals with irregular arrangement appear at a deposition temperature of 800 °C (Figure 4d). Between 850 and 900 °C, the morphology of as-deposited TiO_2 coatings alters to smooth strips and presents the interwoven structures (Figure 4e, f). In addition, the grain size is gradually increasing when the deposition temperature is between 650 and 750 °C, whereas the grain size is not obviously changed between 800 and 900 °C. This demonstrates that deposition temperature has a

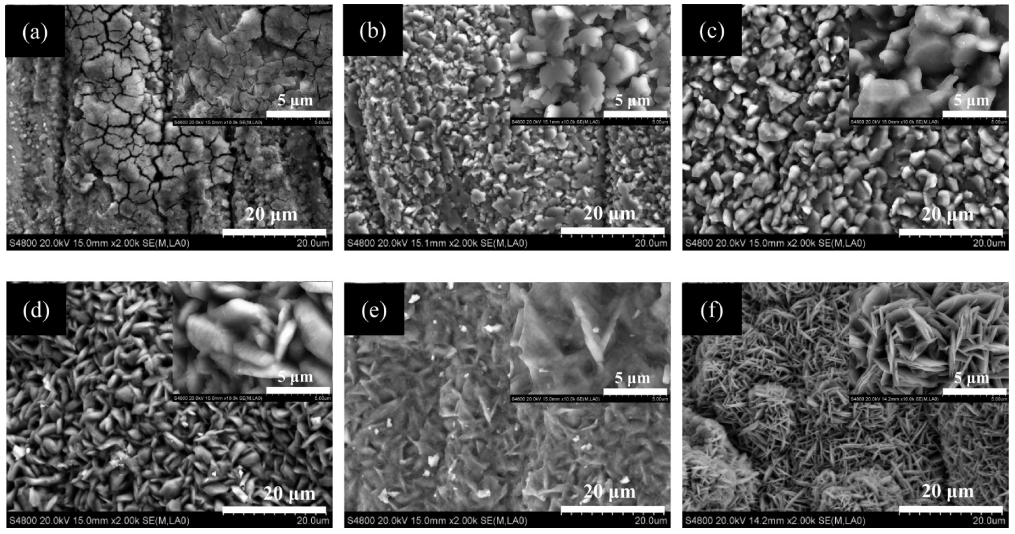

Figure 4. SEM images of TiO_2 coatings at various deposition temperatures: (a) 650, (b) 700, (c) 750, (d) 800, (e) 850, and (f) 900 °C.

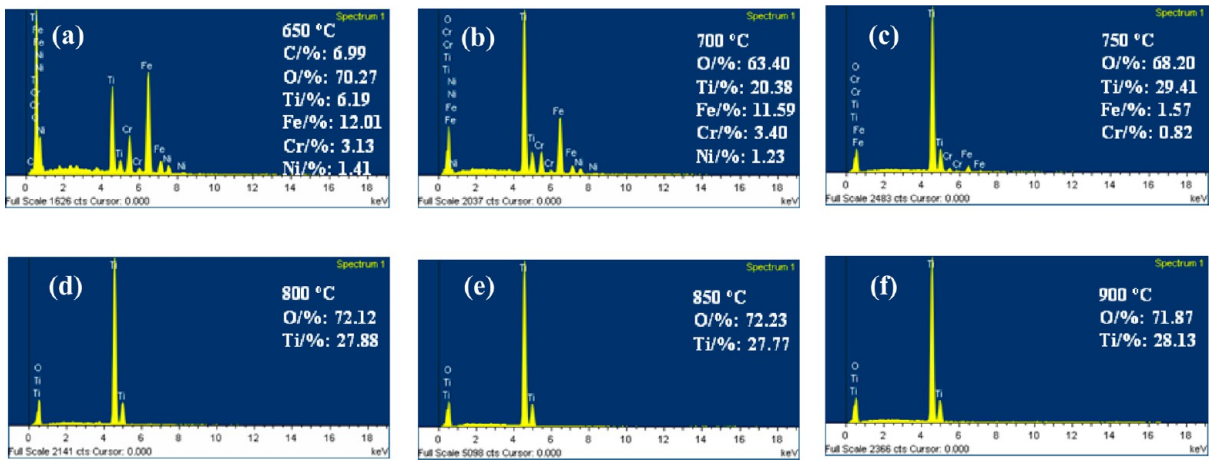

Figure 5. EDX spectra of TiO_2 coatings at different deposition temperatures: (a) 650, (b) 700, (c) 750, (d) 800, (e) 850, and (f) 900 °C.

stronger effect on the morphology or granular shape than the grain size.

It is generally accepted that there are three possible modes of crystal growth on surfaces: (i) the island, or Volmer–Weber mode; (ii) the layer, or Frank-van der Merwe mode; (ii) the layer plus island, or Stranski–Krastanov mode.[32] The morphology of TiO_2 coating growth can be explained by Volmer–Weber mode which happens when the atoms (or molecules) of the deposit are more strongly bound to each other than to the substrate while Frank-van der Merwe mode displays the opposite characteristics. At low deposition temperatures, the growth rate of TiO_2 coating is relatively slow and causes that those cracks and gaps on the SS304 substrate are still visible, and the island structures survive after deposition period of 3 h at 650 °C. At high deposition temperatures, atoms (or molecules) of the deposit are enough activated and nuclei of crystals grow up fast. In this case, the island structures can combine quickly and form a continuous film that leads to the disappearance of the cracks and gaps ultimately. Furthermore, the TiO_2 coatings are more homogeneous and compact above 800 °C. This may indicate that the TiO_2 coatings can cover the SS304 substrate surface completely when the deposition temperature is above 800 °C.

3.2. Elemental Composition of As-Deposited TiO_2 Coatings. Figure 5 presents the EDX spectra of elemental composition evolution of TiO_2-coated tube inner surfaces (100 mm away from gas inlet) with the deposition temperature increasing. All the elemental data are within ±3% percentage error. It can be observed that Fe, Cr and Ni at.% of the substrate gradually changes to 0 when the deposition temperature is up to 800 °C. It is possible that the surface of the substrate cannot be covered by TiO_2 coating completely until the deposition temperature is above 800 °C, or these metal atoms could migrate away from the cracks and gaps under the impetus of temperature gradient. Because of TiO_2 coatings with the same deposition time, it could be also attributed to the thickness of TiO_2 coatings is relatively thin at lower deposition temperatures, therefore, the EDX signal can penetrate the TiO_2 coatings. Further, this clearly indicates these metallic elements are gradually covered by TiO_2 coatings as the deposition temperature increases to 800 °C, which means TiO_2 deposition efficiency is different at different CVD temperature. The higher temperature used the better CVD efficiency. Moreover, the as-deposited TiO_2 coatings show a non-stoichiometric composition and the Ti/O ratio is seldom changed (Ti/O ratio is close to 3:8) when the deposition temperature is above 800 °C. In this regard, the deposition

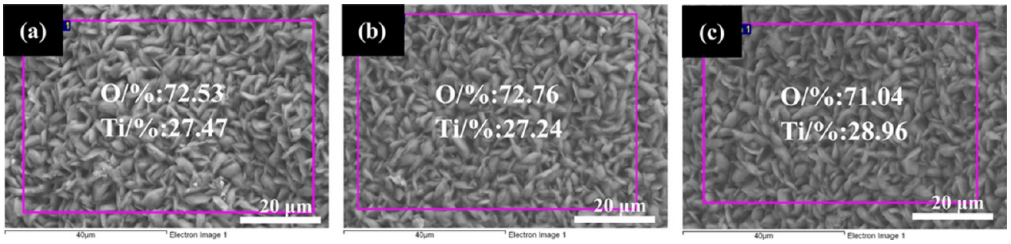

Figure 6. Morphology and elemental composition of different parts of TiO_2 coating at a deposition temperature of 800 °C: (a) 100, (b) 350, and (c) 600 mm.

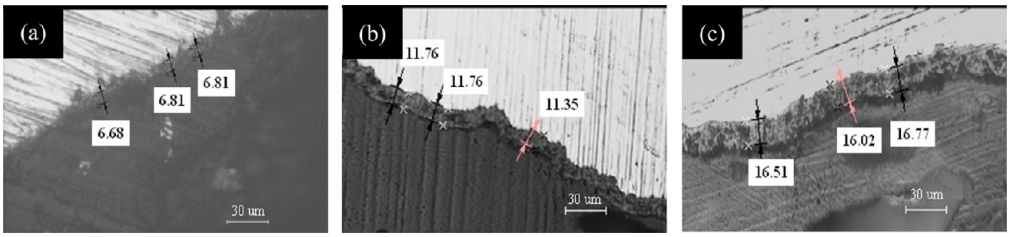

Figure 7. Thickness of TiO_2-coated tube fracture cross-section with different deposition temperature: (a) 800, (b) 850, and (c) 900 °C.

temperature has little influence on the chemical composition of TiO_2 coating at high temperature range. This is further evidence that the TiO_2 coatings can cover the SS304 substrate surface completely when deposition temperature is above 800 °C, which is consistent with the SEM results.

3.3. Uniformity and Thickness of As-Deposited TiO_2 Coatings. Previous morphologies and elemental composition analysis of TiO_2 coatings by SEM and EDX were employed the position of 100 mm away from gas inlet. As shown in Figure 6, to illustrate the uniformity of TiO_2 coatings throughout the inner surface of tubes, three split samples of TiO_2 coated tube at a deposition temperature of 800 °C, for example, were chosen for morphology and elemental composition analysis: 100, 350, and 600 mm along the axial length of the tube. Apparently, rice-shaped crystals with irregular arrangement morphology are exhibited at the whole regions for all parts of as-deposited TiO_2 coating, which also show a nonstoichiometric composition of Ti_3O_8. The results clearly demonstrate that TiO_2 coating is uniform along the tube.

Because of the thermal cracking of hydrocarbon fuels under high temperature and pressure, coating thickness is an important index for anticoking coating applications. Here we only considered the TiO_2 coatings at deposition temperature above 800 °C, which shows no metallic elements detected by EDX to avoid the metal catalytic coking. Figure 7 displays the thickness of TiO_2-coated tube fracture cross sections at the deposition temperature between 800 and 900 °C by metalloscopy. It is clear that TiO_2 coating has a clear interface and uniform thickness at each deposition temperature. The average thickness of TiO_2 coatings is 6.77 μm for 800 °C, 11.62 μm for 850 °C, and 16.43 μm for 900 °C, respectively. This implies that the deposition rate of TiO_2 coating increases linearly from 2.26 μm/h to 5.48 μm/h as the deposition temperature increases from 800 to 900 °C. Kuo et al.[33] have also studied the crystalline titanium oxide films with a thickness of 0.09−0.55 μm at temperatures below 500 °C by means of the $TiCl_4/CO_2/H_2$ process. In their report, they proposed a growth mechanism and showed that the film thickness decreased with increasing substrate temperature and CO_2/H_2 input, and they attributed this to considerable desorption instead of deposition at higher temperature which can be explained by the weak bonding of the film to the substrate. In contrast to their results an increscent film thickness takes place at the higher deposition temperatures in this work. As is known to all, reactions between metal chlorides and water are very fast. In the case of higher deposition temperature, the homogeneous water gas shift reaction (eq 1) in the gas phase has commonly been accepted as the rate-determining step in this process.[34,35] According to eq 3, water formation rate increases as the temperature rises; therefore, the deposition rate also inevitably increases with the increase in temperature.

3.4. Phase Composition of As-Deposited and Annealed TiO_2 Coatings. The crystal phase structures of as-deposited and annealed TiO_2 coatings deposited at 800 °C were analyzed by XRD and shown in Figure 8. It is observed that the as-deposited TiO_2 coating consists of Ti_2O_3 and Ti_3O_5 phases, whereas the annealed TiO_2 coating consists of only rutile TiO_2 (JCPDS card number 21−1276). The (110), (101) and (211) reflections of annealed TiO_2 coating at 2θ angles of

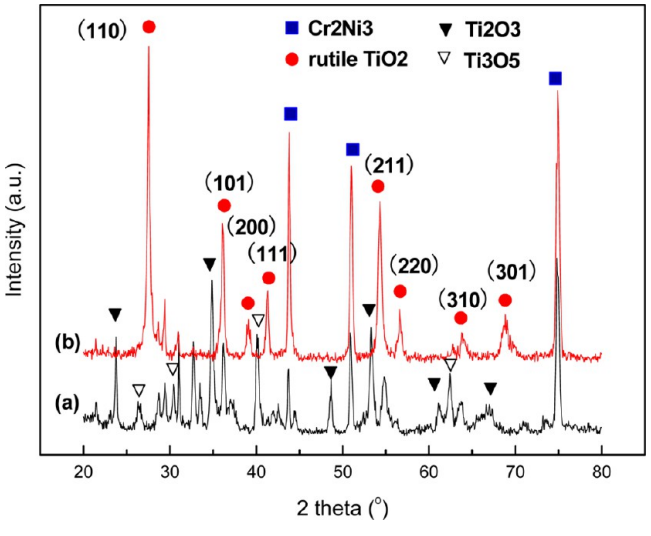

Figure 8. XRD patterns of (a) as-deposited and (b) annealed TiO_2 coatings deposited at 800 °C.

dx.doi.org/10.1021/am5048762 | ACS Appl. Mater. Interfaces 2014, 6, 17157−17165

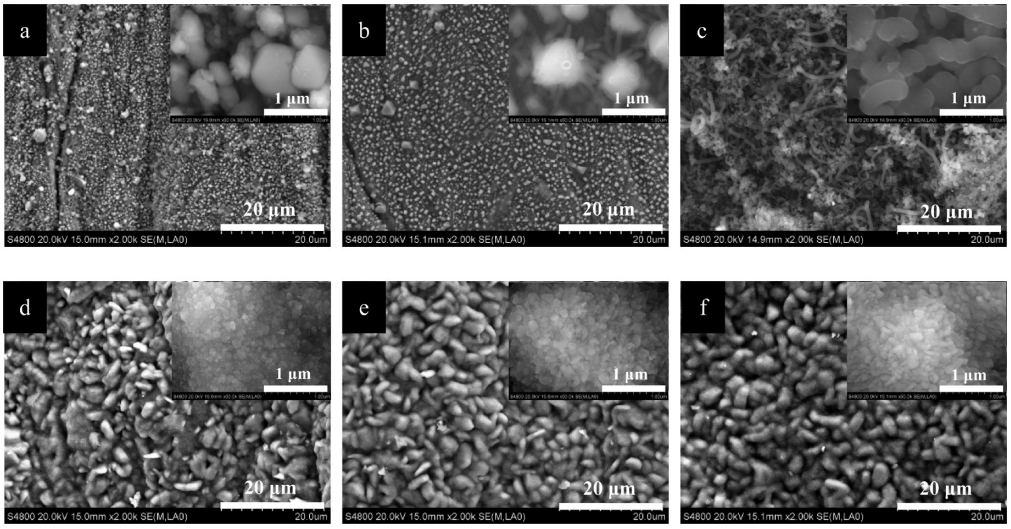

Figure 9. SEM images of the carbon deposits on different parts of isothermal section inner surface of SS304 bare and TiO_2-coated tube: (a) 100 mm of bare tube; (b) 350 mm of bare tube; (c) 600 mm of bare tube; (d) 100 mm of TiO_2-coated tube; (e) 350 mm of TiO_2-coated tube; and (f) 600 mm of TiO_2-coated tube.

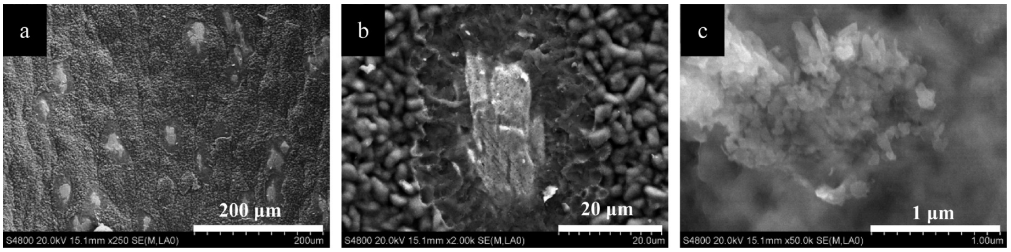

Figure 10. Different magnification SEM images of the partial loss of TiO_2 coating after coking test at the position of 600 mm: (a) 250:1, (b) 2000:1, and (c) 50000:1.

27.6, 36.1, and 54.3° are more pronounced than other diffraction peaks. When the as-deposited TiO_2 coating was annealed at 700 °C for 30 min, a series of obvious diffraction peaks of TiO_2 coating became more relatively narrow and acuity. This implies that the crystal phase structures of annealed TiO_2 coating are relatively complete with a high crystallinity compared to as-deposited TiO_2 coating. Nevertheless, because of the strong penetrating of X-ray, some additional reflections corresponding to the substrate such as Cr_2Ni_3 (JCPDS card number 65−6291) were observed in both as-deposited and annealed TiO_2 coatings. In summary, these results suggest that the as-deposited TiO_2 coating is oxidized completely and obtained a rutile TiO_2 coating after annealing. It is noteworthy to point out that the annealing process changes the phase composition of as-deposited TiO_2 coating but does not change its morphology.

3.5. Anticoking Performance of TiO_2 Coating. Because of the TiO_2 coatings at low temperature with some detected metal atoms, while the thickness of TiO_2 coating is more than 6 μm at a deposition temperature of 800 °C, which is enough to cut off the catalytic coke growth effect of the metal substrate, the anticoking tests were carried out in bare and annealed TiO_2-coated tubes at a deposition temperature of 800 °C. Figure 9 presents SEM images (2000:1) of the carbon deposits on different parts of isothermal section inner surface of SS304 tube and TiO_2 coating after *n*-hexane pyrolysis at 600 °C and 3.3 MPa for 1 h. The morphology evolution of carbon deposits which formed by severe catalytic coking along the axial length of SS304 tube can be clearly seen in Figure 9a−c: (i) a large number of granular deposits which consist of crystallites with sharp edges and 0.2−1 μm sizes appear on 100 mm zone of bare tube. As previous studies,[14,36,37] it is a possibility that these granular deposits belong to metal carbides, such as Fe_3C and Cr_3C; (ii) there are numerous granular deposits on 350 mm zone of bare tube, and Figure 9b is very similar to Figure 9a. Differently, the high-magnification images of the particles show that some whiskers of carbon deposition appear under these granular deposits. This can be attributed to carbon precipitation from metal carbides in the process of the formation of filamentous coke.[38] (iii) As shown in Figure 9c, a lot of interwoven filamentous coke cover cracks and gaps of the substrate completely, and the high-magnification images of the filamentous coke show that the coke diameter is about 316 nm with a coarse skin, which because of the coke precursors in the gas phase react with the coke surface through radical reactions and lateral growth of the filament begins.[39,40] Comparing Figure 9e with f, the morphology of TiO_2 coating along the tube has little changed before and after *n*-hexane pyrolysis at 600 °C and 3.3 MPa for 1 h. However, a lot of amorphous carbon deposits adhere to the surface of TiO_2 grain under high magnification. It suggests that the surface reaction of metal catalytic coking is fully cut off when the surface of metal substrate is completely covered by TiO_2 coating, then the free radical and olefin condensation coking in the bulk phase are dominant in this case. As a conclusion, compared with the corresponding SEM images of bare and TiO_2-coated tube after

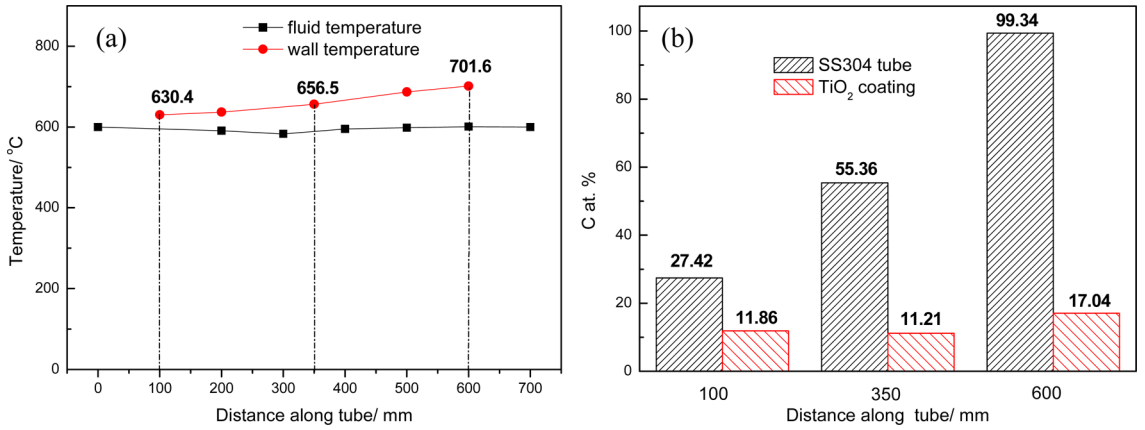

Figure 11. (a) Fluid and wall temperature (T_f and T_w) profiles and (b) C at. % along the reactor tube of isothermal section after *n*-hexane thermal cracking at 600 °C and 3.3 MPa.

coking, it can visually see that the coke on the surface of TiO_2 coating are far less than that on the surface of bare tube. Thus, TiO_2 coating provides a very good protective layer to prevent the substrate from severe coking.

Unfortunately, partial loss was observed at the 600 mm zone of TiO_2 coating surface after coking test, as shown in Figure 10. This may due to the rapid cooling and the weak bonding of the TiO_2 coating to the substrate. Nevertheless, no filamentous coke was observed in the region of the partial loss (see Figure 10b, c). This result implies that the partial loss of TiO_2 coating takes place after coking test instead of in the process of the experiment.

To further illustrate the morphology evolution of coke formation and anticoking performance on TiO_2 coating, the fluid and wall temperatures were measured as Liu et al.[41] described and the carbon in atomic percentage (C at %) of the SS304 substrate and TiO_2 coatings along the tube after coking tests were analyzed by EDX. Figure 11 presents the fluid and wall temperature (T_f and T_w) profiles and C at. % along the reactor tube of isothermal section after *n*-hexane thermal cracking at 600 °C and 3.3 MPa. It can be observed from Figure 11a that the T_f is almost changed and keep at 600 °C while the T_w is gradually increased from the fuel inlet to outlet. The difference between T_f and T_w is less than 110 °C. Figure 11b shows that C at % along the SS304 tube is also gradually increased as the T_w increases, but C at % along the TiO_2-coated tube has little change. On the one hand, it demonstrates that the morphology evolution of coke formation and C at % are closely related to the T_w rather than T_f due to the filamentous coke growth belong to the surface reaction. On the other hand, the results again indicate that TiO_2 coating can play an important part in preventing the metal substrate from catalytic coking effectively.

The carbon mass distribution of coke along the axial length of isothermal section of the tube and the anticoking ratio (calculated by eq 4) of TiO_2 coating are compiled in Figure 12. It is clear that the carbon mass of coke on the surface of bare tube is higher than that on the surface of TiO_2-coated tube. Due to some coke formation and accumulation in the joint of two ends, carbon mass of the two 5 cm segments at both ends of the joint is not the true carbon mass of coke on the inner surface of reaction tubes (denoted as ellipses). Generally, the carbon mass of both bare and TiO_2-coated tube roughly increases gradually along the axial length of tube, which is consistent with the results of the T_w. In addition, the results of

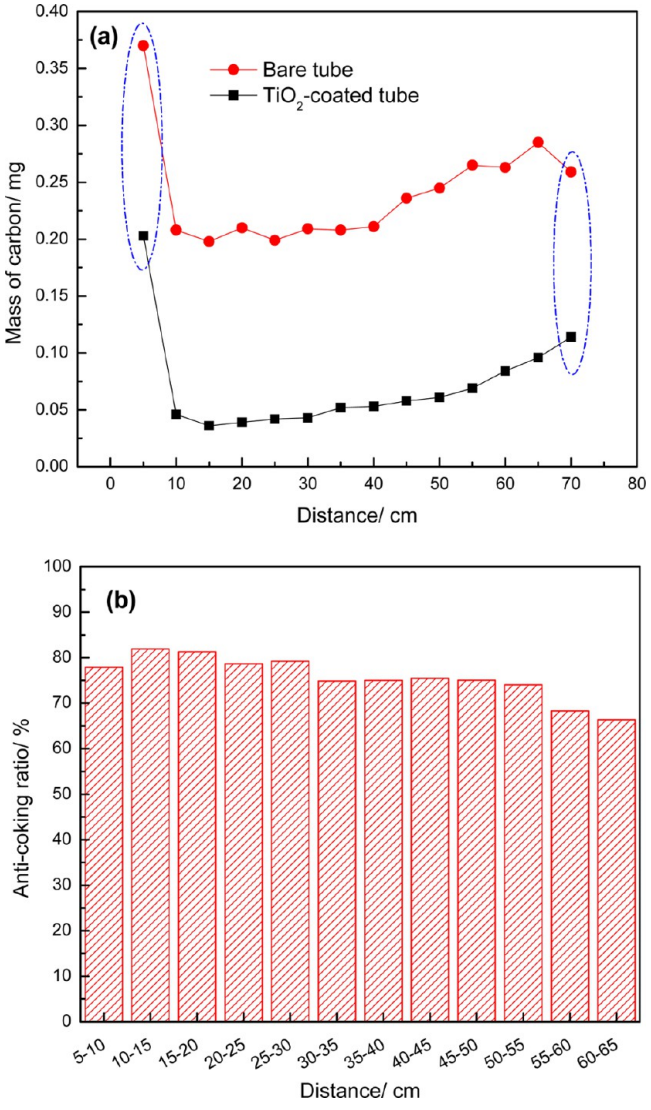

Figure 12. (a) Carbon mass distribution of coke along the axial length of isothermal section of the bare and TiO_2-coated tubes, and (b) the anticoking ratio of TiO_2 coating along the tube.

the anticoking ratio of TiO_2 coating corresponding to each 5 cm segments show that the anticoking ratio of TiO_2 coating is above 65% and the average anticoking ratio of TiO_2 coating is

dx.doi.org/10.1021/am5048762 | ACS Appl. Mater. Interfaces 2014, 6, 17157−17165

up to 76% (Figure 12b). Therefore, the results further confirm that TiO_2 coating displays a good anticoking performance and provides a good protective layer to prevent the substrate from metal dusting and severe coking.

4. CONCLUSIONS

TiO_2 coatings were prepared on the inner surface of SS304 tube in a horizontal hot-wall reactor at atmospheric pressure by thermal CVD method using the $TiCl_4/CO_2/H_2$ process at various substrate temperatures ranging from 650 to 900 °C. The rutile TiO_2 coating was obtained by annealing the as-deposited TiO_2 coating, which is an alternative route for the deposition of rutile TiO_2 coatings. The deposition temperature has a strong effect on the morphology and thickness of as-deposited TiO_2 coatings. In particular, small particles and island structures with many cracks and gaps can be seen on the surface of as-deposited TiO_2 coating at a deposition temperature of 650 °C. Irregular platelike crystals appear at the deposition temperatures of 700 and 750 °C. Rice-shaped crystals with irregular arrangement appear at a deposition temperature of 800 °C. Between 850 and 900 °C, the morphology of TiO_2 coatings alters to smooth strips and presents the interwoven structures. The grain size is gradually increasing when the deposition temperature is increased from 650 to 750 °C, whereas the grain size is not obviously changed between 800 and 900 °C. When the deposition temperature is above 800 °C, the thickness of TiO_2 coating is more than 6 μm and uniform, and the films have a nonstoichiometric composition of Ti_3O_8.

The anticoking performance of rutile TiO_2 coating was evaluated by *n*-hexane pyrolysis at 600 °C and 3.3 MPa for 1 h. The TiO_2 coating at a deposition temperature of 800 °C is sufficiently thick to cover the cracks and gaps on the surface of the substrate and cut off the catalytic coke growth effect resulting from the metal substrate. As a conclusion, compared with the corresponding SEM images of bare and TiO_2-coated tube, it can visually see carbon deposits on the surface of TiO_2 coating are far less than that on the surface of SS304 tube. The anticoking ratio of TiO_2 coating corresponding to each 5 cm segments is above 65% and the average anticoking ratio of TiO_2 coating is up to 76%. Thus, the TiO_2 coating can provide a very good protective layer to prevent the substrate from severe coking efficiently.

AUTHOR INFORMATION

Corresponding Authors

*E-mail: wangjianli@scu.edu.cn. Phone/Fax: +86-28-85418451.

*E-mail: yqchen@scu.edu.cn

Notes

The authors declare no competing financial interest.

ACKNOWLEDGMENTS

This research was performed in the Key Laboratory of Green Chemistry and Technology of the Ministry of Education, College of Chemistry, Sichuan University. The research was supported by the National Natural Science Foundation of China (Grants 91016002, J1103315 and J1310008), Outstanding Young Scholar Fund of Sichuan University (Grant 2013SCU04A05), and Program for New Century Excellent Talents in University of Ministry of Education of China (NCET-13-0398).

REFERENCES

(1) Pang, H.; Yang, H.; Guo, C. X.; Li, C. M. Functionalization of SnO_2 photoanode through Mg-doping and TiO_2-coating to synergically boost dye-sensitized solar cell performance. *ACS Appl. Mater. Interfaces* **2012**, *4*, 6261−6265.

(2) Su, Y.; Zhang, X.; Han, S.; Chen, X.; Lei, L. F−B-codoping of Anodized TiO_2 Nanotubes Using Chemical Vapor Deposition. *Electrochem. Commun.* **2007**, *9*, 2291−2298.

(3) Hitchman, M. L.; Tian, F. Studies of TiO_2 Thin Films Prepared by Chemical Vapour Deposition for Photocatalytic and Photoelectrocatalytic Degradation of 4-Chlorophenol. *J. Electroanal. Chem.* **2002**, *538*−*539*, 165−172.

(4) Wang, Z.; Hu, X. Fabrication and Electrochromic Properties of Spin-coated TiO_2 Thin Films from Peroxo-polytitanic Acid. *Thin Solid Films* **1999**, *352*, 62−65.

(5) Ren, M.; Yin, H.; Lu, Z.; Wang, A.; Yu, L.; Jiang, T. Evolution of Rutile TiO_2 Coating Layers on Lamellar Sericite Surface Induced by Sn^{4+} and the Pigmentary Properties. *Powder Technol.* **2010**, *204*, 249−254.

(6) Chuang, L.; Luo, C.; Yang, S. The Structure and Mechanical Properties of Thick Rutile−TiO_2 Films Using Different Coating Treatments. *Appl. Surf. Sci.* **2011**, *258*, 297−303.

(7) Li, C. S.; Yang, Y. S. A Glass Based Coating for Enhancing Anticoking and Anti-carburizing Abilities of Heat-resistant Steel HP. *Surf. Coat. Technol.* **2004**, *185*, 68−73.

(8) Yang, C.; Liu, G.; Wang, X.; Jiang, R.; Wang, L.; Zhang, X. Preparation and Anticoking Performance of MOCVD Alumina Coatings for Thermal Cracking of Hydrocarbon Fuels under Supercritical Conditions. *Ind. Eng. Chem. Res.* **2012**, *51*, 1256−1263.

(9) Mohan, A. R.; Eser, S. Effectiveness of Low-Pressure Metal−Organic Chemical Vapor Deposition Coatings on Metal Surfaces for the Mitigation of Fouling from Heated Jet Fuel. *Ind. Eng. Chem. Res.* **2011**, *50*, 7290−7304.

(10) Zhou, J.; Wang, Z.; Luan, X.; Xu, H. Anti-coking Property of the SiO_2/S Coating During Light Naphtha Steam Cracking in a Pilot Plant Setup. *J. Anal. Appl. Pyrolysis* **2011**, *90*, 7−12.

(11) Zhou, J.; Xu, H.; Liu, J.; Qi, X.; Zhang, L.; Jiang, Z. Study of Anti-coking Property of SiO_2/S Composite Coatings Deposited by Atmospheric Pressure Chemical Vapor Deposition. *Mater. Lett.* **2007**, *61*, 5087−5090.

(12) Wang, Z.; Xu, H.; Zhou, J.; Luan, X. Simulation of SiO_2/S Coating Deposition in a Pilot Plant Set-up for Coking Inhibition. *Chem. Eng. Res. Des.* **2013**, *91*, 120−133.

(13) Tang, S.; Gao, S.; Wang, S.; Wang, J.; Zhu, Q.; Chen, Y.; Li, X. Characterization of CVD TiN Coating at Different Deposition Temperatures and Its Application in Hydrocarbon Pyrolysis. *Surf. Coat. Technol.* **2014**, http://dx.doi.org/10.1016/j.surfcoat.2014.07.029.

(14) Tang, S.; Gao, S.; Hu, S.; Wang, J.; Zhu, Q.; Chen, Y.; Li, X. Inhibition Effect of APCVD Titanium Nitride Coating on Coke Growth during n-Hexane Thermal Cracking under Supercritical Conditions. *Ind. Eng. Chem. Res.* **2014**, *53*, 5432−5442.

(15) Tang, S.; Hu, S.; Zhang, Y.; Wang, J.; Zhu, Q.; Chen, Y.; Li, X. Influence of TiN Coating on Products Distribution for Hydrocarbon Fuel Cracking under High Temperature and Pressure. *J. Anal. Appl. Pyrolysis* **2014**, *107*, 197−203.

(16) Ervin, J. S.; Ward, T. A.; Williams, T. F.; Bento, J. Surface Deposition within Treated and Untreated Stainless Steel Tubes Resulting from Thermal-Oxidative and Pyrolytic Degradation of Jet Fuel. *Energy Fuels* **2003**, *17*, 577−586.

(17) Van Bui, H.; Groenland, A. W.; Aarnink, A. A. I.; Wolters, R. A. M.; Schmitz, J.; Kovalgin, A. Y. Growth Kinetics and Oxidation Mechanism of ALD TiN Thin Films Monitored by In Situ Spectroscopic Ellipsometry. *J. Electrochem. Soc.* **2011**, *158*, H214−H220.

(18) Kim, D.; Seong, T.; Baik, Y. Oxidation Behavior of TiN/AlN Multilayer Films Prepared by Ion Beam-assisted Deposition. *Thin Solid Films* **2001**, *397*, 203−207.

(19) Barshilia, H. C.; Rajam, K. S. Raman Spectroscopy Studies on the Thermal Stability of TiN, CrN, TiAlN Coatings and Nanolayered

TiN/CrN, TiAlN/CrN Multilayer Coatings. *J. Mater. Res.* **2004**, *19*, 3196−3205.
(20) Deng, B.; Tao, Y.; Zhu, X.; Qin, H. The Oxidation Behavior and Tribological Properties of Si-implanted TiN Coating. *Vacuum* **2014**, *99*, 216−224.
(21) Yu, J.; Zhao, X.; Zhao, Q.; Wang, G. Preparation and Characterization of Super-hydrophilic Porous TiO_2 Coating Films. *Mater. Chem. Phys.* **2001**, *68*, 253−259.
(22) Wang, W.; Li, S.; Wen, Y.; Gong, M.; Zhang, L.; Yao, Y.; Chen, Y. Synthesis and Characterization of $TiO_2/YFeO_3$ and Its Photocatalytic Oxidation of Gaseous Benzene. *Acta Phys.-Chim. Sin.* **2008**, *24*, 1761−1766.
(23) Melero, H.; Torrell, M.; Fernández, J.; Gomes, J. R.; Guilemany, J. M. Tribological Characterization of Biocompatible HAp-TiO_2 Coatings Obtained by High Velocity Oxy-fuel Spray. *Wear* **2013**, *305*, 8−13.
(24) Zhang, X.; Hang, R.; Wu, H.; Huang, X.; Ma, Y.; Lin, N.; Yao, X.; Tian, L.; Tang, B. Synthesis and Antibacterial Property of Ag-containing TiO_2 Coatings by Combining Magnetron Sputtering with Micro-arc Oxidation. *Surf. Coat. Technol.* **2013**, *235*, 748−754.
(25) Byun, D.; Jin, Y.; Kim, B.; Kee Lee, J.; Park, D. Photocatalytic TiO_2 Deposition by Chemical Vapor Deposition. *J. Hazard. Mater.* **2000**, *73*, 199−206.
(26) Kaliwoh, N.; Zhang, J.; Boyd, I. W. Characterisation of TiO_2 Deposited by Photo-induced Chemical Vapour Deposition. *Appl. Surf. Sci.* **2002**, *186*, 241−245.
(27) Zhang, X.; Zhou, M.; Lei, L. Preparation of Anatase TiO_2 Supported on Alumina by Different Metal Organic Chemical Vapor Deposition Methods. *Appl. Catal., A* **2005**, *282*, 285−293.
(28) Guo, D.; Ito, A.; Goto, T.; Tu, R.; Wang, C.; Shen, Q.; Zhang, L. Effect of Laser Power on Orientation and Microstructure of TiO_2 Films Prepared by Laser Chemical Vapor Deposition Method. *Mater. Lett.* **2013**, *93*, 179−182.
(29) Sun, H.; Wang, C.; Pang, S.; Li, X.; Tao, Y.; Tang, H.; Liu, M. Photocatalytic TiO_2 Films Prepared by Chemical Vapor Deposition at Atmosphere Pressure. *J. Non-Cryst. Solids* **2008**, *354*, 1440−1443.
(30) Fredriksson, E.; Carlsson, J. Chemical Vapour Deposition of TiO and Ti_2O_3 from $TiCl_4/H_2/CO_2$ Gas Mixtures. *Surf. Coat. Technol.* **1995**, *73*, 160−169.
(31) Tingey, G. L. Kinetics of the Water—Gas Equilibrium Reaction. I. The Reaction of Carbon Dioxide with Hydrogen. *J. Phys. Chem.* **1966**, *70*, 1406−1412.
(32) Venables, J. A.; Spiller, G.; Hanbucken, M. Nucleation and Growth of Thin Films. *Rep. Prog. Phys.* **1984**, *47*, 399.
(33) Kuo, D.; Shueh, C. Growth and Properties of $TiCl_4$-Derived CVD Titanium Oxide Films at Different CO_2/H_2 Inputs. *Chem. Vap. Deposition* **2003**, *9*, 265−271.
(34) Lux, B.; Colombier, C.; Altena, H.; Stjernberg, K. Preparation of Alumina Coatings by Chemical Vapour Deposition. *Thin Solid Films* **1986**, *138*, 49−64.
(35) Mårtensson, P. Influence of the Concentration of $ZrCl_4$ on Texture, Morphology and Growth Rate of CVD Grown α-Al_2O_3 Coatings Deposited by the $AlCl_3/ZrCl_4/H_2/CO_2/H_2S$ Process. *Surf. Coat. Technol.* **2006**, *200*, 3626−3632.
(36) Altin, O.; Eser, S. Analysis of Solid Deposits from Thermal Stressing of a JP-8 Fuel on Different Tube Surfaces in a Flow Reactor. *Ind. Eng. Chem. Res.* **2001**, *40*, 596−603.
(37) Altin, O.; Eser, S. Characterization of Carbon Deposits from Jet Fuel on Inconel 600 and Inconel X Surfaces. *Ind. Eng. Chem. Res.* **2000**, *39*, 642−645.
(38) Zeng, Z.; Natesan, K. Relationship between the Growth of Carbon Nanofilaments and Metal Dusting Corrosion. *Chem. Mater.* **2005**, *17*, 3794−3801.
(39) Wang, Z.; Xu, H.; Luan, X.; Hou, F.; Zhou, J. Effect of Potassium Acetate on Coke Growth during Light Naphtha Thermal Cracking. *Ind. Eng. Chem. Res.* **2011**, *50*, 10292−10297.
(40) Mohamadalizadeh, A.; Towfighi, J.; Karimzadeh, R. Modeling of Catalytic Coke Formation in Thermal Cracking Reactors. *J. Anal. Appl. Pyrolysis* **2008**, *82*, 134−139.
(41) Jiang, R.; Liu, G.; Zhang, X. Thermal Cracking of Hydrocarbon Aviation Fuels in Regenerative Cooling Microchannels. *Energy Fuels* **2013**, *27*, 2563−2577.